Published for SISSA by Springer

Received: *January 8, 2018*
Accepted: *February 16, 2018*
Published: *March 14, 2018*

Polarized double-virtual amplitudes for heavy-quark pair production

L. Chen,[a] **M. Czakon**[b] **and R. Poncelet**[b]

[a] *Werner-Heisenberg-Institut, Theoretical Physics Division, Max-Planck Institute for Physics, Föhringer Ring 6, München, D-80805 Germany*

[b] *Institute for Theoretical Particle Physics and Cosmology, RWTH Aachen University, Aachen, D-52056 Germany*

E-mail: longchen@mpp.mpg.de, mczakon@physik.rwth-aachen.de, poncelet@physik.rwth-aachen.de

Abstract: We present the two-loop virtual amplitudes for heavy-quark pair production in light quark-antiquark annihilation and gluon fusion channels, including full spin and color dependence. We use expansions around kinematical limits and numerical integration to obtain results for the involved master integrals. From these, we determine the renormalised infrared finite remainders of the coefficients of amplitude decompositions in terms of color and spin structures. The remainders are given in form of numerical interpolation grids supported by expansions around the production threshold and the high energy limit. Finally, we provide the spin density matrix, which encodes the heavy-quark spin correlations and is sufficient for phenomenological applications. Our results are necessary for the derivation of top-quark pair production cross sections in hadron collisions in the narrow width approximation with next-to-next-to-leading order accuracy in QCD.

Keywords: QCD Phenomenology

ArXiv ePrint: 1712.08075

https://doi.org/10.1007/JHEP03(2018)085

JHEP03(2018)085

Contents

1 Introduction

The top-quark is the heaviest known particle and measurements of its properties provide important insights into the Standard Model of Particle Physics and beyond. Top-quark pair production at hadron colliders like the LHC or Tevatron is an important process for Standard Model precision measurements as well as searches for new physics. Considering the hadronic production of stable top-quark pairs, the prediction from Quantum Chromodynamics (QCD) is compelete to next-to-next-to leading order (NNLO) for the total cross section [1] and for differential distributions [2–4]. More recently NLO corrections from electroweak interactions [5, 6] were also incorporated. A more complete modelling of pair production including decay and off-shell effects is available to NLO accuracy in QCD [7, 8] in the case of the di-lepton channel and more recently also for the semi-leptonic channel [10]. These results were extended to pair production in association with a jet [11, 12], which is of relevance for inclusive production at NNLO.

Corrections to the top-quark decay process are known through NNLO in QCD [13, 14]. This has allowed for a partial prediction of the pair-production differential cross sections with decay modelled within the Narrow Width Approximation (NWA) [15]. The only missing piece of information is the exact contribution from NNLO production followed by LO decay of the top quarks. This requires the knowledge of polarised two-loop amplitudes for this process, which is the subject of this publication.

The evaluation of the polarised two-loop amplitudes closely follows the lines of [16]. To obtain spin and color dependence of the amplitudes, we use projection techniques, which

JHEP03(2018)085

were also successfully applied in various two-loop calculations, for instance [17]. The most demanding part of this calculation is the reduction and evaluation of involved scalar integrals. The appearing scalar integrals can be reduced to the same set of master integrals as those involved in the evaluation of the spin-summed amplitude. The evaluation of these master integrals uses a variety of analytical and numerical techniques. Exploiting the system of differential equations obeyed by these master integrals is the core idea behind these methods. Most of the physical phase space region can be accessed by solving the differential equations numerically. The regions of phase space that contain physical singularities cannot be reliably accessed using numerical integration. We perform deep power-logarithmic expansions around these singularities in order to obtain precise values for the master integrals. We provide the results in terms of an expansion around the production threshold, a high energy expansion, as well as an interpolation grid. To present and discuss some features of our results, we recast the obtained coefficients with respect to a basis in color and spin space, in terms the spin density matrix of the top quarks alone. Although our results are obtained with numerical methods, there is also progress in the analytic evaluation of master integrals for this process [18–22].

This paper is organised in the following way. In the next section we define the spin and color structures into which the amplitudes are decomposed. We also discuss the projection method we used to obtain the coefficients. Afterwards, we describe the methods used to obtain numerical values for the master integrals in the physical phase space region as well as the improvements we made considering the choice of the master integral basis. Next, we present and discuss the results for the obtained coefficients. We close with conclusions and outlook.

2 Structure of the amplitude

2.1 Spin and color structures for virtual amplitudes

The production of heavy quark pairs at hadron-hadron colliders involves two partonic QCD processes at lowest multiplicity

$$gg \to Q\bar{Q} \qquad \text{and} \qquad q\bar{q} \to Q\bar{Q}\,. \tag{2.1}$$

The momenta are assigned as follows

$$g, q(p_1) + g, \qquad \bar{q}(p_2) \to t(p_3) + \bar{t}(p_4)\,, \tag{2.2}$$

with on-shell conditions

$$p_1^2 = p_2^2 = 0\,, \qquad p_3^2 = p_4^2 = m_t^2\,. \tag{2.3}$$

We define the following kinematic invariants

$$s \equiv (p_1 + p_2)^2\,, \qquad t \equiv m_t^2 - (p_1 - p_3)^2\,, \qquad u \equiv m_t^2 - (p_2 - p_3)^2\,, \tag{2.4}$$

where the relation $s - t - u = 0$ holds as a consequence of the aforementioned on-shell conditions and momentum conservation. These invariants are related to the scattering

JHEP03(2018)085

angle θ of the top quark (with respect to the beam axis in p_1 direction) and the top quark velocity β as

$$t = \frac{s}{2}\left(1 - \beta\cos\theta\right) , \qquad u = \frac{s}{2}\left(1 + \beta\cos\theta\right) , \qquad \text{with} \quad \beta = \sqrt{1 - 4\frac{m_t^2}{s}} . \tag{2.5}$$

The bare scattering amplitude can be expanded in a perturbative series in $\alpha_s = g_s^2/4\pi$ and reads up to second order

$$|\mathcal{M}_{g,q}(\alpha_s, m_t, \epsilon)\rangle = 4\pi\alpha_s \left[\left|\mathcal{M}^{(0)}_{g,q}(m_t,\epsilon)\right\rangle + \left(\frac{\alpha_s}{2\pi}\right)\left|\mathcal{M}^{(1)}_{g,q}(m_t,\epsilon)\right\rangle + \left(\frac{\alpha_s}{2\pi}\right)^2 \left|\mathcal{M}^{(2)}_{g,q}(m_t,\epsilon)\right\rangle \right] . \tag{2.6}$$

To facilitate the calculation of polarized virtual amplitudes, we decompose them in terms of color and spin (Lorentz) structures in the color $\otimes$ spin space of external particles.

The color and spin decompositions of virtual amplitudes can be written as

$$\left|\mathcal{M}^{(l)}_{g,q}(m_t,\epsilon)\right\rangle = \sum_{i,j} c^{(l)}_{ij}(m_t, s, t, \epsilon)\, |C^{g,q}_i\rangle \otimes |S^{g,q}_j\rangle , \tag{2.7}$$

where l = number of loops, and the $|C^{g,q}_i\rangle$, $|S^{g,q}_j\rangle$ on the right-hand side represent, respectively, the chosen basis structures in the color $\otimes$ spin space. We denote the state of the external particles by $|a,b,c,d\rangle$ in color and $|h_1,h_2,h_3,h_4\rangle$ in spin space, where a,b and h_1,h_2 concern the initial state, while c,d and h_3,h_4 the final state, in the same order as for the kinematics. With this notation, the color and spin basis structures of eq. (2.7) can be written in full generality in the case of a gluon initial state as

$$\begin{aligned} \langle a,b,c,d|C^g_i\rangle &= (C^g_i)^{ab}_{cd} , \\ \langle h_1,h_2,h_3,h_4|S^g_i\rangle &= \epsilon_1(h_1)_\mu \epsilon_2(h_2)_\nu \bar{u}_3(h_3)(S_i)^{g\mu\nu} v_4(h_4) , \end{aligned} \tag{2.8}$$

and similarly for a quark initial state

$$\begin{aligned} \langle a,b,c,d|C^q_i\rangle &= (C^q_i)_{abcd} , \\ \langle h_1,h_2,h_3,h_4|S^q_i\rangle &= \bar{v}_2(h_2)\Gamma_i u_1(h_1)\bar{u}_3(h_3)\Gamma'_i v_4(h_4) . \end{aligned} \tag{2.9}$$

Notice that in our work, we do not choose any specific representation of spinors or polarisation vectors. Thus, for example, $h_{3,4}$ are not necessarily helicities in the case of the heavy quarks. By providing results in terms of spin structures S_i, we allow to translate the amplitudes to any particular polarisation basis. For phenomenological applications, we provide the spin density matrix, which contains all the necessary information in terms of spin vectors of the heavy quarks, see section 2.3.

The color decomposition basis of amplitudes can be chosen straightforwardly. For the $gg \to t\bar{t}$, we use the natural basis

$$\begin{aligned} C^g_1 &= (T^a T^b)_{cd} , \\ C^g_2 &= (T^b T^a)_{cd} , \\ C^g_3 &= \mathrm{Tr}\{T^a T^b\}\delta_{cd} . \end{aligned} \tag{2.10}$$

In the case of quark annihilation in the initial state, the color basis reads

$$C_1^q = \delta_{ab}\delta_{cd}\,,$$
$$C_2^q = \delta_{ad}\delta_{cb}\,. \tag{2.11}$$

For each of the color structures C_i, we decompose the amplitudes further in terms of spin (Lorentz) structures. To this end, we assume that all four external particles are confined to 4-dimensional space and are on-shell with physical polarization states (i.e. 4-dimensional equations of motion are satisfied). Under this condition, we have in total $2^4 = 16$ different physical helicity configurations both in the $gg \to t\bar{t}$ and the $q\bar{q} \to t\bar{t}$ process. Additional symmetry properties enjoyed by the amplitudes can lead to relations which further reduce the number of linearly independent structures. Indeed, on top of the aforementioned kinematic constraints, QCD interactions are invariant with respect to parity, under which the helicity of each of the four external particles is flipped, while the color structures are left unchanged. This symmetry then reduces the linearly independent spin structures down to 8 (in 4-dimensional space), both in the $gg \to t\bar{t}$ and $q\bar{q} \to t\bar{t}$ cases. QCD interactions are also invariant under charge conjugation. However, this operation also involves the color structure. For this reason, we did not impose C-symmetry when determining the basis of Lorentz structures for the color-stripped amplitudes. For the same reason, implications from Bose-symmetry between the two gluons are not considered at this point, but rather used as a test at the end of the calculation.

At this point, we discuss the particulars for the two specific amplitudes, since additional symmetry properties are process dependent.

Let us first consider the $gg \to t\bar{t}$ case. Here, we assume that both polarisation vectors are orthogonal to both of the initial state momenta, p_1 and p_2 (see eq. (2.2)). This reduces the number of degrees of freedom to the physical two. Spin sums should, therefore, be performed with

$$\sum_{\mathrm{h}} \epsilon_\mu^*(h)\epsilon_\nu(h) = \left(-g_{\mu\nu} + \frac{p_{1\mu}p_{2\nu} + p_{1\nu}p_{2\mu}}{p_1 \cdot p_2}\right)\,. \tag{2.12}$$

After stripping off the external wave functions we choose the following set of 8 Lorentz structures, with suppressed spinor indices

$$S_1^{g\mu\nu} = \frac{1}{s}\left(\gamma^\mu p_3^\nu + \gamma^\nu p_3^\mu\right)\,, \qquad S_2^{g\mu\nu} = \frac{m_t}{s}\, g^{\mu\nu}\mathbf{1}\,,$$
$$S_3^{g\mu\nu} = \frac{1}{s\, m_t}\, p_3^\mu\, p_3^\nu \mathbf{1}\,, \qquad S_4^{g\mu\nu} = \frac{1}{s\, m_t^2}\, \not{p}_1 p_3^\mu p_3^\nu\,,$$
$$S_5^{g\mu\nu} = \frac{1}{s}\, \not{p}_1 g^{\mu\nu}\,, \qquad S_6^{g\mu\nu} = \frac{1}{s\, m_t}\, \not{p}_1 \left(\gamma^\nu p_3^\mu + \gamma^\mu p_3^\nu\right)\,,$$
$$S_7^{g\mu\nu} = \frac{1}{s}\left(\gamma^\mu p_3^\nu - \gamma^\nu p_3^\mu\right)\,, \qquad S_8^{g\mu\nu} = \frac{m_t}{s}\left(\not{p}_1 g^{\mu\nu} - \not{p}_1 \gamma^\mu \gamma^\nu\right)\,. \tag{2.13}$$

The additional factors of m_t and s are inserted such that all structures are dimensionless once multiplied with spinors (which are assumed to have mass dimension 1/2). The structures are grouped according to whether they are symmetric (S_1 to S_6) or anti-symmetric

JHEP03(2018)085

(S_7 and S_8) under the exchange of $\mu \leftrightarrow \nu$. It can be checked explicitly that each of the above Lorentz structures is mapped back to itself under the parity transformation (up to a phase factor). The Gram determinant of this set of structures is not identically zero, assuring that they are linearly independent.

In case of the $q\bar{q} \to t\bar{t}$ process with massless initial-state quarks and limited to QCD interactions, the massless quark line is disconnected from the massive top-quark line. Chirality conservation in QCD, therefore, implies that only half of the helicity configurations of the initial-state massless quarks are non-zero. Once this additional constraint is accounted on top of those aforementioned ones, one finds that there are only four independent helicity amplitudes left. We therefore choose the following set of 4 Lorentz structures of the form $S = \Gamma \otimes \Gamma'$ (Γ denotes a string of γ matrices)

$$S_1^q = \frac{1}{s\, m_t} \not{p}_3 \otimes \mathbf{1} \,, \quad S_2^q = \frac{1}{s\, m_t^2} \not{p}_3 \otimes \not{p}_1 \,, \quad S_3^q = \frac{1}{s} \gamma^\mu \otimes \gamma_\mu \,, \quad S_4^q = \frac{1}{s\, m_t} \gamma^\mu \otimes (\not{p}_1 \gamma_\mu) \,, \tag{2.14}$$

where the left-hand side of the $\otimes$ symbol concerns the massless fermion line, while the right-hand side concerns the massive fermion line. Again, the linear independence of these structures can be verified via the Gram determinant.

The coefficient functions of the above color and spin decomposition of amplitudes can be extracted by performing the usual projection procedure. In short, the projection of the virtual amplitude onto each of the chosen basis structures gives an equation linear in the coefficient functions. The collection of all projections onto the linearly independent, complete set of basis structures then forms an invertible linear algebraic equation system in the coefficient functions, which can be solved straightforwardly. The coefficient matrix of this linear algebraic equation system is identical to the Gram matrix of the chosen basis.

We note already at this point that in our calculation, the structures S_6^g and S_4^q have vanishing coefficients for all color structures.

Even though we performed our calculations with the basis specified in eq. (2.10), it is possible to express the coefficient functions for the gluon channel in terms of the orthonormal basis

$$C_{\mathbf{8_S}}^g = \sqrt{\frac{2N_C}{(N_C^2-1)(N_C^2-4)}} \left(C_1^g + C_2^g - \frac{2}{N_C} C_3^g \right) , \tag{2.15}$$

$$C_{\mathbf{8_A}}^g = \sqrt{\frac{2}{N_C(N_C-1)}} \left(C_1^g - C_2^g \right) , \tag{2.16}$$

$$C_{\mathbf{1}}^g = \frac{2}{\sqrt{N_C(N_C-1)}} C_3^g \,, \tag{2.17}$$

where $N_C = 3$ is the number of colors, and $\mathbf{8_S}$, $\mathbf{8_A}$ denote the symmetric and anti-symmetric octet states respectively, while $\mathbf{1}$ the singlet state. The advantage of this choice of basis is that there is no mixing between the color structures when calculating color summed amplitudes. On the other hand, with these structures the coefficient functions exhibit a simple Bose symmetry. Indeed, for the spin structures $S_1^{g\,\mu\nu}$, $S_2^{g\,\mu\nu}$, $S_3^{g\,\mu\nu}$, $S_7^{g\,\mu\nu}$, $S_8^{g\,\mu\nu}$ the coefficients of $C_{\mathbf{8_S}}^g$ and $C_{\mathbf{1}}^g$ are symmetric under the exchange $\cos\theta \to -\cos\theta$, while the

coefficient of $C^g_{\mathbf{8_A}}$ is anti-symmetric under this transformation. For the spin structures $S_4^{g\,\mu\nu}$ and $S_5^{g\,\mu\nu}$ the situation is reversed, the coefficients of $C^g_{\mathbf{8_S}}$ and $C^g_{\mathbf{1}}$ are anti-symmetric while $C^g_{\mathbf{8_A}}$ have symmetric coefficients. These properties are consistent with the numerical results, and constitute a test of the calculation.

2.2 Ultraviolet and infrared renormalisation

The chosen color $\otimes$ spin basis may be used in d-dimensions after extension of the spin structures by evanescent combinations. For physical applications, however, we should only need 4-dimensional quantities. Due to the presence of infrared singularities, meaningful amplitudes are only obtained after the usual ultraviolet renormalisation followed by infrared subtraction (multiplicative renormalisation). This procedure results in so-called finite remainders, which are, however, scheme dependent.

The UV renormalized amplitude reads

$$\left|\mathcal{M}^R_{g,q}(\alpha_s^{(n_f)}, m, \mu, \epsilon)\right\rangle = \left(\frac{\mu^2 e^{\gamma_E}}{4\pi}\right)^{-2\epsilon} Z_{g,q} Z_Q \left|\mathcal{M}^0_{g,q}(\alpha_s^0, m^0, \epsilon)\right\rangle , \tag{2.18}$$

where we used the on-shell wave function renormalisation constants Z_g, Z_q and Z_Q. The renormalised heavy quark mass m is related to the bare mass by $m^0 = Z_m m$. The coupling constant is renormalized in the $\overline{\text{MS}}$ scheme with $n_f = n_l + n_h$ active flavours

$$\alpha_s^0 = \left(\frac{e^{\gamma_E}}{4\pi}\right)^{\epsilon} \mu^{2\epsilon} Z_{\alpha_s}^{(n_f)} \alpha_s^{(n_f)}(\mu) . \tag{2.19}$$

As argued in [16] a decoupling of the heavy flavours from the running of α_s is necessary to correctly accommodate for heavy quark mass effects in regimes where the produced heavy quarks are not very relativistic. This decoupling can be achieved by the replacement

$$\alpha_s^{(n_f)} = \zeta_{\alpha_s} \alpha_s^{(n_l)} , \tag{2.20}$$

where ζ_{α_s} is the decoupling constant.

The wave-function and the coupling renormalisation (including decoupling) act multiplicatively on the amplitudes and, therefore, also on the coefficients c_{ij}. The mass renormalization counter term, on the other hand, requires an additional decomposition of the lower order amplitudes into color $\otimes$ spin structures. The necessary renormalisation and decoupling constants are given in the appendix A.

The UV renormalized coefficient functions still contain infrared divergences. However, the infrared structure is known in terms of lower order amplitudes [23–29], and can be extracted from the UV renormalised amplitude

$$\left|\mathcal{M}_n^{(0)}\right\rangle = \left|\mathcal{F}_n^{(0)}\right\rangle \quad , \tag{2.21}$$

$$\left|\mathcal{M}_n^{(1)}\right\rangle = \mathbf{Z}^{(1)} \left|\mathcal{M}_n^{(0)}\right\rangle + \left|\mathcal{F}_n^{(1)}\right\rangle \quad , \tag{2.22}$$

$$\left|\mathcal{M}_n^{(2)}\right\rangle = \mathbf{Z}^{(2)} \left|\mathcal{M}_n^{(0)}\right\rangle + \mathbf{Z}^{(1)} \left|\mathcal{F}_n^{(1)}\right\rangle + \left|\mathcal{F}_n^{(2)}\right\rangle \tag{2.23}$$

$$= \left(\mathbf{Z}^{(2)} - \mathbf{Z}^{(1)}\mathbf{Z}^{(1)}\right) \left|\mathcal{M}_n^{(0)}\right\rangle + \mathbf{Z}^{(1)} \left|\mathcal{M}_n^{(1)}\right\rangle + \left|\mathcal{F}_n^{(2)}\right\rangle , \tag{2.24}$$

JHEP03(2018)085

where $|\mathcal{F}_n\rangle$ is the finite remainder amplitude, we are interested in. $\mathbf{Z} = \mathbf{1} + \mathbf{Z}^{(1)} + \mathbf{Z}^{(2)} + \mathcal{O}(\alpha_s{}^3)$ is the IR renormalization constant. It is an operator in color space and can be obtained from its renormalisation group equation

$$\frac{\mathrm{d}}{\mathrm{d}\ln\mu_R}\mathbf{Z}\left(\epsilon,\{p_i\},\{m_i\},\mu_R\right) = -\mathbf{\Gamma}\left(\{p_i\},\{m_i\},\mu_R\right)\mathbf{Z}\left(\epsilon,\{p_i\},\{m_i\},\mu_R\right) , \tag{2.25}$$

where the anomalous dimension $\mathbf{\Gamma}$ is given in the appendix A. Since the $\mathbf{Z}$ operator acts in color-space, the terms $\mathbf{Z}^{(i)}\left|\mathcal{M}_n^{(k)}\right\rangle$ have to be projected back onto the color structures to obtain the corresponding counter terms for the coefficients. The minimal definition of the renormalisation operator $\mathbf{Z}$, which consists of poles in the dimensional regularisation parameter only, specifies our IR renormalisation scheme uniquely.

In [61], it was shown that the triple-color correlators of the soft anomalous dimension matrix cannot contribute to spin and color summed matrix elements. Since we keep color and spin dependence this is no longer true in our case. In fact, our calculation is the first to rely on the coefficient

$$\sum_{(I,J)}\sum_{k} i\, f^{abc}\,\mathbf{T}_I^a\,\mathbf{T}_J^b\,\mathbf{T}_k^c\, f_2\left(\beta_{IJ}, \ln\frac{-\sigma_{Jk}\, v_J\cdot p_k}{-\sigma_{Ik}\, v_I\cdot p_k}\right) ,$$

to correctly obtain all poles of the coefficients functions. In consequence, it constitutes the first non-trivial cross-check of this contribution to the soft anomalous dimension matrix, which was originally derived in [28].

2.3 Spin density matrix

For illustration of our results, we choose to recast the amplitude into a more convenient form. In general, since each coefficient has a real and imaginary part, our calculation yields 54 real functions. However, not all of them enter independently into physical predictions. Therefore, we also evaluate the spin density matrix, which contains all the necessary information on the top-quark spin dependence and is sufficient for phenomenological applications.

The spins of the top-quarks in their rest frame can be described by two normalised spin 3-vectors $\hat{\mathbf{s}}_t$ and $\hat{\mathbf{s}}_{\bar{t}}$. They correspond to two four-vectors s_t and $s_{\bar{t}}$ in the center of mass frame which have the properties

$$s_t^2 = s_{\bar{t}}^2 = -1 \qquad \text{and} \qquad p_3\cdot s_t = p_4\cdot s_{\bar{t}} = 0 . \tag{2.26}$$

The vectors s_t and $s_{\bar{t}}$ enter the matrix element through the insertion of the spin projectors

$$u(p_3,s_t)\bar{u}(p_3,s_t) = \left(\not{p}_3 + m\right)\frac{1}{2}\left(1+\gamma_5\not{s}_t\right) , \tag{2.27}$$

$$v(p_4,s_{\bar{t}})\bar{v}(p_4,s_{\bar{t}}) = \left(\not{p}_4 - m\right)\frac{1}{2}\left(1+\gamma_5\not{s}_{\bar{t}}\right) . \tag{2.28}$$

Since we work with finite remainders without any divergences, the presence of the γ_5 matrix does not constitute any complication. Indeed, the spin density matrix is simply evaluated

JHEP03(2018)085

in 4 dimensions. The two-loop contribution to the spin-density matrix for both partonic processes can be decomposed as

$$\begin{aligned}\mathcal{R}^{\text{2-loop}}_{q,g}(s_t, s_{\bar{t}}) = \; & 2\,\mathrm{Re}\left\langle \mathcal{M}^0_{q,g} \middle| \mathcal{M}^2_{q,g} \right\rangle (s_t, s_{\bar{t}}) = A_{q,g} + (C)_{q,g}\left((s_t \cdot s_{\bar{t}})\right) \\ & + (B_t)_{q,g}\left(\epsilon^{\mu\nu\alpha\beta} p_{1\mu} p_{2\nu} p_{3\alpha} s_{t\beta}\right) + (B_{\bar{t}})_{q,g}\left(\epsilon^{\mu\nu\alpha\beta} p_{1\mu} p_{2\nu} p_{3\alpha} s_{\bar{t}\beta}\right) \\ & + (D_1)_{q,g}\left((p_1 \cdot s_t)(p_1 \cdot s_{\bar{t}})\right) + (D_2)_{q,g}\left((p_2 \cdot s_t)(p_2 \cdot s_{\bar{t}})\right) \\ & + (E_{12})_{q,g}\left((p_1 \cdot s_t)(p_2 \cdot s_{\bar{t}})\right) + (E_{21})_{q,g}\left((p_2 \cdot s_t)(p_1 \cdot s_{\bar{t}})\right). \end{aligned} \tag{2.29}$$

These functions are related to the 2-loop components of the spin density matrix $R^{q,g}$ as defined in [51] through

$$\mathcal{R}^{\text{2-loop}}_{q,g} = \frac{1}{4}\,\mathrm{Tr}\left[R^{q,g}(\mathbf{1} + \hat{\mathbf{s}}_t\sigma) \otimes (\mathbf{1} + \hat{\mathbf{s}}_{\bar{t}}\sigma)\right]\Big|_{\text{2-loop}}. \tag{2.30}$$

The coefficients of the occurring structures are functions of $\cos\theta$ and β only. In pure QCD C,P and CP invariance hold and imply that $B_t = B_{\bar{t}} = B$ as well as $D_1 = D_2 = D$ [51] for both channels. Therefore we are left with

$$\begin{aligned}\mathcal{R}^{\text{2-loop}}_{q,g} = \; & A_{q,g} + (B)_{q,g}\left(\epsilon^{\mu\nu\alpha\beta} p_{1\mu} p_{2\nu} p_{3\alpha} s_{t\beta} + \epsilon^{\mu\nu\alpha\beta} p_{1\mu} p_{2\nu} p_{3\alpha} s_{\bar{t}\beta}\right) \\ & + (C)_{q,g}\left((s_t \cdot s_{\bar{t}})\right) + (D)_{q,g}\left((p_1 \cdot s_t)(p_1 \cdot s_{\bar{t}}) + (p_2 \cdot s_t)(p_2 \cdot s_{\bar{t}})\right) \\ & + (E_{12})_{q,g}\left((p_1 \cdot s_t)(p_2 \cdot s_{\bar{t}})\right) + (E_{21})_{q,g}\left((p_2 \cdot s_t)(p_1 \cdot s_{\bar{t}})\right). \end{aligned} \tag{2.31}$$

In the gluon case we have an additional bose-symmetry which implies that the functions A_g, C_g, D_g are symmetric in $\cos\theta$ and that B_g has to be an antisymmetric function in $\cos\theta$. It also implies the relation $E_{12g}(\cos\theta) = E_{21g}(-\cos\theta)$.

3 Scalar integrals

The coefficients functions c_{ij} are given by linear combinations of a large number of scalar integrals with rational coefficients in s, t, m^2 and ϵ. These scalar integrals are expressed through linear combinations of master integrals using an Integration-by-Parts (IBP) reduction. We can rewrite the coefficients, as well as the master integrals, in terms of dimensionless variables $m_s = m^2/s$ and $x = t/s$. From the IBP relations we can obtain a system of differential equations for the master integrals

$$m_s \frac{\partial}{\partial m_s}\vec{I}(m_s, x, \epsilon) = A^{(m_s)}(m_s, x, \epsilon)\vec{I}(m_s, x, \epsilon)\,, \tag{3.1}$$

$$x \frac{\partial}{\partial x}\vec{I}(m_s, x, \epsilon) = A^{(x)}(m_s, x, \epsilon)\vec{I}(m_s, x, \epsilon)\,, \tag{3.2}$$

where $A^{(m_s)}$ and $A^{(x)}$ are matrices whose elements are rational functions in m_s, x and ϵ.

JHEP03(2018)085

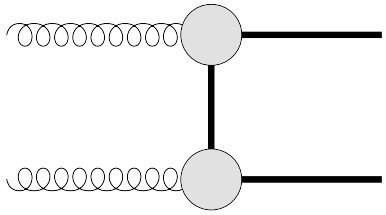

Figure 1. Class of diagrams leading to enhanced matrix elements at high energy and low scattering angle.

We do not choose the same set of master integrals as in the spin summed calculation. There is an enhancement of the matrix elements at high energies and small/large scattering angles resulting from diagrams of a t/u-channel type as indicated in figure 1. These enhancements require numerically very stable results for the master integrals in these phase space regions. For this reason, we decided to try a basis for a subset of the integrals, which corresponds to the ϵ-form of the differential equation (see next section). Our hope was that in this basis the numerical evaluation will become more stable. Ultimately, this turned out not to be the case. We stress, nevertheless, that the results obtained in the old and new bases for the spin summed amplitudes agree to several digits, within the accuracy of the calculation.

3.1 Canonicalization

With the hope to achieve a better stability when numerically solving the differential equations for master integrals involved in the two-loop $gg \to t\bar{t}$ process, we choose to put the equation system partially into the ϵ-form [30], where the right-hand side of the differential equation system is proportional to $\epsilon = \frac{d-4}{2}$ and the singularities are only simple poles in the kinematic variables. Algorithmic approaches have been devised to arrive at the ϵ-form for a given differential equation system for master-integrals in a single variable [31, 32]. They have been implemented in Fushsia [34] and Epsilon [35] which are publicly available. In the case of multiple variables there also exists an algorithm, presented in refs. [36, 37] and implemented in a program called Canonica. It is well known that, for a given set of master integrals, an ϵ-form is not always achievable by a rational transformation of the integral basis. It is also not always possible [32, 38, 39] even with more general transformations. In particular, ref. [32] provides a strict criterion for the existence of an ϵ-form in the case of master integrals of a single variable. In particular, the 4-dimensional homogeneous part of the differential equation system typically corresponds to high-order Picard-Fuchs differential equations that do not factorize completely [39]. The simplest counter example is given by the differential equations of the master integrals of the two-loop sunset diagrams with identical masses [40, 41], where solutions involve elliptic integrals.

The topology of the two-loop sunset diagrams with equal masses appears in the IBP-reduction of the master integrals of the two-loop $gg \to t\bar{t}$ diagrams. Thus, it is not a surprise that the full system of differential equations of the 422 master integrals involved cannot be completely put into the ϵ-form. In addition, a considerable amount of sectors

JHEP03(2018)085

require individual coordinate transformations in order to arrive at their respective ϵ-forms by rational transformations (in the new variables). Since we would like to numerically integrate the full differential equation system of all master integrals in one go, we are then forced to divide the master integrals into two subsets: those that can be directly put into the ϵ-form via a rational transformation in the original variables and those that cannot. The second subset essentially consists of master integrals fulfilling any of the following three conditions:

1) their expressions involve elliptic integrals;

2) coordinate transformations are required in order to reach their ϵ-form;

3) their derivatives involve any one of the aforementioned two kinds of master integrals.

Under such tight selection criteria, there are only 65 master integrals that can be directly transformed into the basis observing the ϵ-form (in the original variables). They are identified and then subsequently moved to the front of the differential equation system of the 422 master integrals, without spoiling the block-wise triangular structure of the differential equation system. The numerical evaluation of the complicated master integrals are expected to benefit from the ϵ-form of these 65 master integrals. The differential equation system of these 65 master integrals in question involves more than one variable,[1] and we employ the package CANONICA [37] to find the rational transformation matrix needed for obtaining the ϵ-form. A few modifications of the program were made in order to tackle this 65-by-65 system with less time consumption.

As a side remark, we would like to briefly mention the following point. Due to the existence of *remnant* rational transformations that preserve the ϵ-form of a differential equation system, the new basis integrals defined by the rational transformation matrix returned by the package CANONICA [37] are not guaranteed to be of uniform weight [30, 38]. Upon a closer examination, we find that in general not all of these remnant rational transformations respecting the ϵ-form (if it exists) are of weight 0 according to the counting rules laid in [30, 38].

To be more specific about this, we find this remnant freedom to be the following. Under any rational transformation mixed with any coordinate-transformation under the condition of keeping the resulting differential system still rational in the new variables, the *remnant* rational transformations that preserve the ϵ-form of the differential equation system (assuming it exists and is represented by $\epsilon \mathrm{d}\tilde{A}$), read

$$\hat{T}_R(\epsilon) = \hat{T}_I(\epsilon)\hat{C}\,, \tag{3.3}$$

where $\hat{C}$ can be any invertible constant matrix of rational numbers of the same dimension as the ϵ-form coefficient-matrix $\mathrm{d}\tilde{A}$. $\hat{T}_I(\epsilon)$ is independent of kinematics but possibly possesses some non-trivial ϵ-dependence. It can be any element from the invariance symmetry group of the coefficient-matrix $\mathrm{d}\tilde{A}$ with matrix elements being Laurent-polynomials in ϵ with rational numerical coefficients. In other words, $\hat{T}_I(\epsilon)$ is a matrix that is invertible and

[1] We treat the triangle graphs as part of box topologies. In principle, one could single out this class of graphs and solve them separately. In this case, there is a basis in which they only depend on one variable. We were interested in trying canonicalization in the multivariate case.

JHEP03(2018)085

commutes with $\mathrm{d}\tilde{A}$ with all its matrix-elements living in the ring of ϵ over rational numbers. Owing to its invertibility and the fact that it consists of rational numbers only, the matrix $\hat{C}$ always preserves the uniform weight feature of the vector on which it acts (if this feature is there in the first place). However, some of $\hat{T}_I(\epsilon)$ with non-trivial ϵ-dependence can turn a list of uniform weight master-integrals into a list of non-uniform-weight integrals, and vice versa, even though both perfectly observe ϵ-form differential equations. Since there is no reference to the concrete boundary conditions of the differential equations in the process of finding the rational transformation done by the package CANONICA, it is therefore not guaranteed that the solutions of the ϵ-form differential equations thus obtained are of uniform weight.

3.2 Master integral evaluation

We subdivide the physical phase space region into three regions, the high energy limit where $m_s \to 0$, the threshold region $\beta \to 0$, and the "bulk" which describes the rest of the phase space region.

For the numerical integration of the new set of master integrals, high precision boundaries are needed. They are obtained from the power-logarithmic expansion in the high energy limit from the original set of master integrals. The first few terms of those expansions were obtained with Mellin-Barns techniques using the MB package [46]. These expansions are exact in t, where in some cases the differential equations were used to get the exact behaviour from the limit $t = 0$. In this double limit $m^2 \to 0$ and $t \to 0$ the integrals were evaluated numerically with very high precision and then resummed with PSLQ algorithm [47] or XSummer [48]. These first terms were used to derive deep expansions in m_s by using the available differential equations. These deep expansions were subsequently used to compute high precision boundaries for the numerical integration.

Starting from the numerical results obtained from the deep power logarithmic expansion, we perform a numerical integration along contours in the complex plane. In our programs we incorporate software from [49] for solving the differential equations and [50] to handle higher precision numbers. The endpoints of the contours define an interpolation grid. In the region which is accessible with this method, i.e. where the coefficient functions are not too singular, we evaluate the amplitudes using this interpolation grid. The sampling points are the same as in [1, 52–54] with an extension to higher values of β.

In the limit $\beta \to 0$ some master integrals show singular behavior and are difficult to obtain with the method of numerical integration. We perform a deep power-logarithmic expansion of the master integrals in β by again exploiting the differential equations up to $\mathcal{O}(\beta^{50})$ and $\mathcal{O}(\ln^{10}\beta)$. This expansion is done for several fixed angles $\cos\theta$ with unknown boundary conditions, which are finally determined by matching to the results obtained by numerical integration.

4 Results

In this publication, we provide results for the finite remainders of all coefficient functions. They are given in the form of an interpolation grid as well as kinematic expansions in the high energy limit and near the production threshold. The decomposition into the structure

JHEP03(2018)085

coefficients yields maximal flexibility since they are independent of the frame, definition of heavy quark spin vectors and other conventions.

At tree-level we find the following non-vanishing coefficients in case of gluons

$$c_{11}^{(0)} = \frac{-1}{x}\,, \qquad c_{21}^{(0)} = \frac{-1}{1-x}\,, \tag{4.1}$$

$$c_{15}^{(0)} = \frac{2x-1}{x}\,, \qquad c_{25}^{(0)} = \frac{2x-1}{1-x}\,, \tag{4.2}$$

$$c_{17}^{(0)} = c_{18}^{(0)} = -c_{11}^{(0)}\,, \qquad c_{27}^{(0)} = c_{28}^{(0)} = -c_{21}^{(0)}\,. \tag{4.3}$$

These have the expected symmetry properties under the replacement $\cos\theta \to -\cos\theta$ or $x \to 1-x$. In case of quark-anti-quark annihilation we find only

$$c_{13}^{(0)} = \frac{1}{2}\,, \qquad c_{23}^{(0)} = \frac{-1}{6}\,, \tag{4.4}$$

to be non-vanishing. We find that in both cases, quark and gluon initial state, one spin structure has vanishing coefficients for every color structure at one and two-loops. Indeed, in the case of gluons the coefficients c_{i6} vanish, as do the coefficients c_{i4} in the case of quarks. All other spin structures have non-vanishing coefficients.

The high energy limit of the coefficients was calculated as an analytic power-logarithmic expansion in $m_s = \frac{m_t}{s}$ up to $\mathcal{O}(m_s^4)$, using the boundary expressions for the master integrals. This expansion assumes that $t, u \gg m_t^2$ and is therefore not valid in the region of high-energy forward/backward scattering. The results were cross-checked against the spin summed amplitude.

We want to mention that the depth of the expansion does not translate easily to the expansion depth of the square summed or spin correlated matrix element since there is a non trivial dependence on m_s (or β in case of the threshold expansion) hidden in the spin structures themselves.

The "bulk" region is parameterized on a grid which is specified by equally spaced points in β

$$\beta_i = i/80\,, \qquad i \in [1, 79]\,, \tag{4.5}$$

and two additional points close to the high energy boundary. The point $\beta_{80} = 0.999$ is sufficient for LHC with 8 TeV center-of-mass energy, which was the extent of the interpolation grid of the spin summed calculation. Here, we extend the grid to $\beta_{81} = 0.9997$ which corresponds to a center of mass energy of 14 TeV, for contemporary applications. For $\cos\theta$ we choose 42 points obtained from

$$\cos\theta = \pm x_i\,, \qquad i \in [1, 21]\,, \tag{4.6}$$

where we chose the x_i as the 21 points obtained from the Gauss-Kronrod integration rule of degree 10. Values for $\beta < 0.1$ were obtained from the threshold expansion of the master integrals. The dependence on the number of light fermions is kept.

JHEP03(2018)085

In order to illustrate our results we plot the coefficients of the spin density matrix. We introduce the following normalization factors, which were also used for the presentation of the results in [16]

$$N_g = \frac{\beta(1-\beta^2)}{4096\pi} \qquad \text{and} \qquad N_q = \frac{\beta(1-\beta^2)}{576\pi}\,, \tag{4.7}$$

and define

$$\mathcal{R}_g^F = N_g 2\,\mathrm{Re}\left\langle \mathcal{M}_g^0 | \mathcal{F}_g^2 \right\rangle (s_t, s_{\bar{t}})\,, \tag{4.8}$$

$$\mathcal{R}_q^F = N_q 2\,\mathrm{Re}\left\langle \mathcal{M}_q^0 | \mathcal{F}_q^2 \right\rangle (s_t, s_{\bar{t}})\,, \tag{4.9}$$

which have the same decomposition as in eq. (2.31). The coefficient functions of $\mathcal{R}_g^F$ and $\mathcal{R}_q^F$ are visualised in figures 2 and 3 for $n_l = 5$. The function $A_{q,g}^{n_l=5}$ is the spin-summed and averaged two-loop finite remainder and was checked against the result from [16]. The function $B_{q,g}^{n_l=5}$ describes the transverse polarization of the top quarks resulting from absorptive parts of the amplitude. At tree-level, this coefficient vanishes due to the absence of complex couplings in QCD. At higher orders, the non-vanishing imaginary part of the virtual amplitudes yields non-zero coefficients. The remaining functions encode the spin correlations between the top and anti-top quark since their structures contain both spin vectors. In the gluon channel, all expected symmetry properties under $\cos\theta \to -\cos\theta$ of the coefficient functions are clearly fulfilled.

The threshold region is covered by points obtained from the deep power-logarithmic expansions of the master integrals. In addition we perform a power-log expansion in β for all coefficients up to β^2. This is done for different but fixed scattering angles $\cos\theta$

$$c_{ij}(\beta, \cos\theta_n) = \sum_{k=-2}^{2} \sum_{l=0}^{2} \tilde{c}_{ij,kl,n} \beta^k \ln^l \beta\,.$$

The dependence on θ was recovered by performing a fit for each set $\{\tilde{c}_{ij,kl,n}\}_n$ to a polynomial $\tilde{c}_{ij,kl} = \sum_{n=0}^{2+k} a_n \cos^n\theta$ separately for the real and imaginary part. The results are also available in electronic format together with this paper. This expansion was used to determine the corresponding coefficients of the spin density matrix as well. Up to $\mathcal{O}(\beta^0)$ we reproduce the analytic result obtained for the spin-summed case in [16].

To study the quality and convergence of the expansion, we also calculated the density matrix for a fixed angle (chosen to be the point x_9) up to order $\mathcal{O}(\beta^6)$. In figures 4 and 5 we compare this expansion against the results obtained from the interpolation grid. We show the difference[2]

$$\left(X_{\text{diff}}^{n_l=5}\right)(\beta, x_9) = \left(X_{\text{thres}}^{n_l=5}\right)(\beta, x_9) - \left(X_{\text{grid}}^{n_l=5}\right)(\beta, x_9)\,, \tag{4.10}$$

with $X \in \{A_g, B_g, C_g, D_g, E_{12g}\}$ for different expansion depths of $\left(X_{\text{thres}}^{n_l=5}\right)(\beta, x_9)$. The series seems to converge nicely and, if expanded up to $\mathcal{O}(\beta^6)$, provides a reasonable description of the amplitude in the region $\beta < 0.3$.

[2]We do not plot the relative difference, because the coefficient functions have a zero in the plotted region.

JHEP03(2018)085

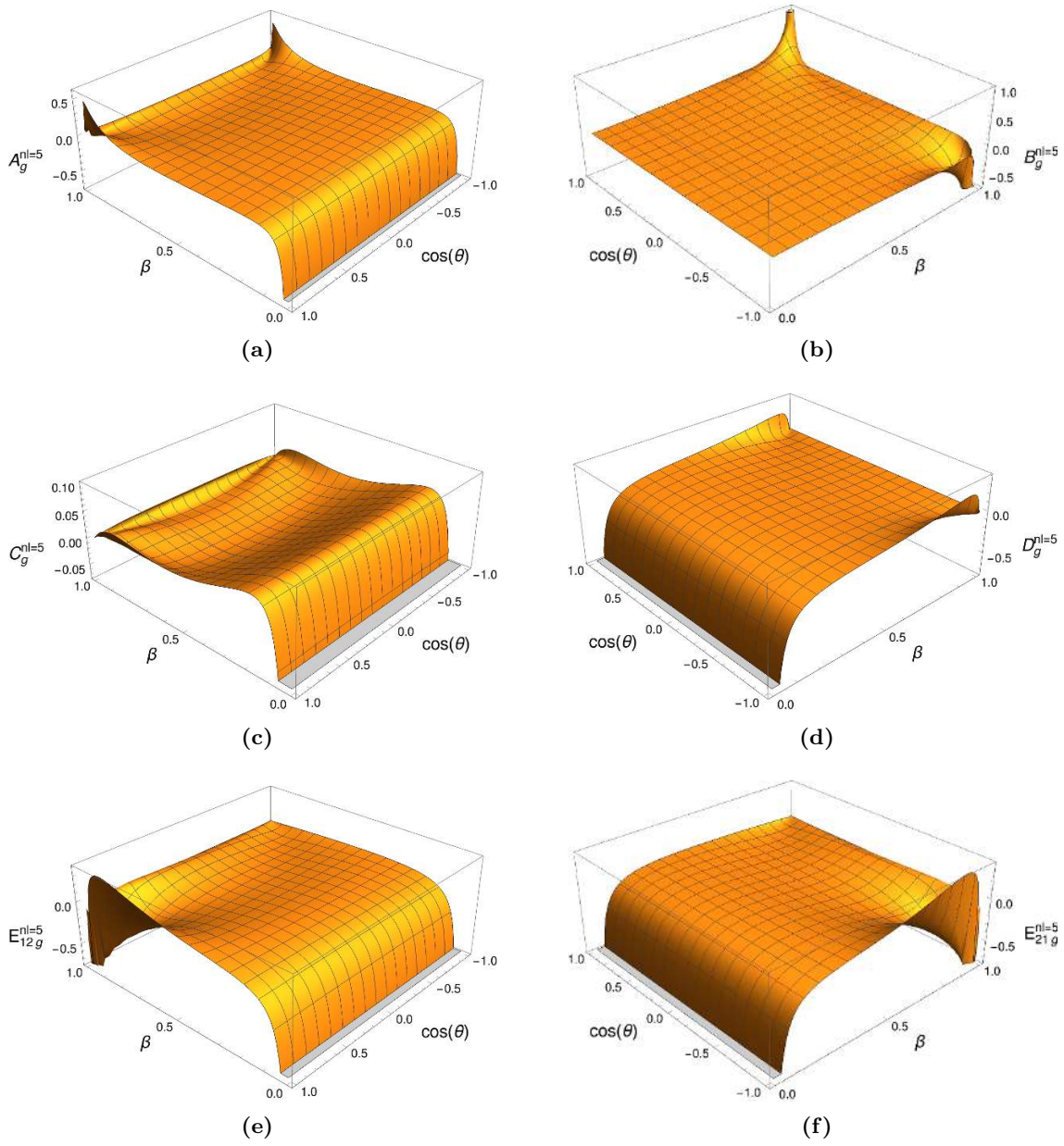

Figure 2. Finite remainder coefficient functions of the spin-density matrix in case of initial state gluons for $n_l = 5$.

5 Conclusions and outlook

We presented the decomposition of the heavy-quark pair production amplitude in terms of spin and color structures at two-loop level. We provide results in terms of interpolation grids and kinematic expansions for these coefficients. As a first application we calculated the spin-density matrix for top-quark pairs. With this work we provide the missing piece needed for the calculation of on-shell top-quark pair production and decay at NNLO in QCD including spin-correlation effects in the narrow width approximation. We improved the numerical results obtained for the involved master integrals by changing to a partly

JHEP03(2018)085

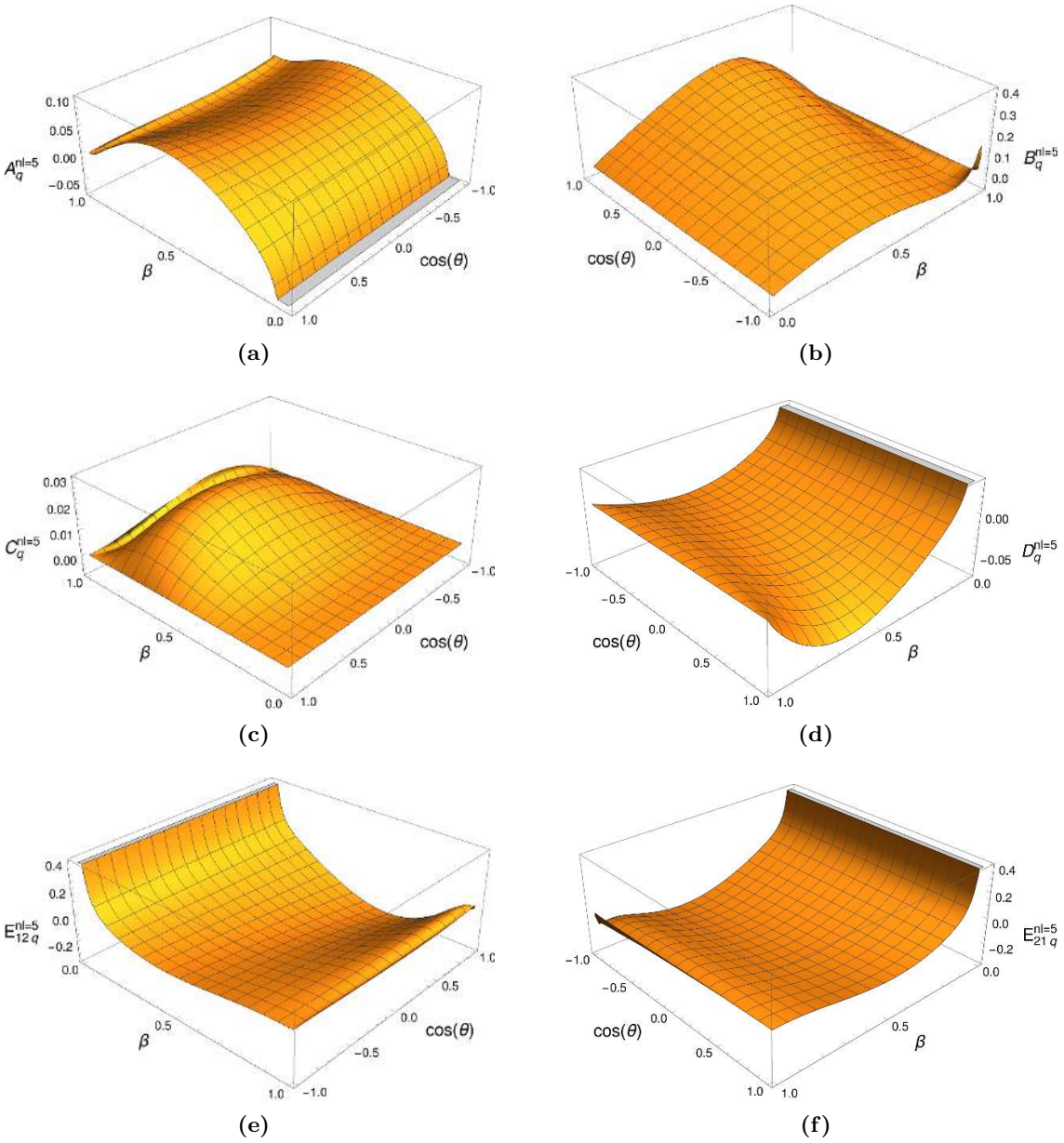

Figure 3. Finite remainder coefficient functions of the spin-density matrix in case of initial state quarks for $n_l = 5$.

canonical basis. The incorporation of these amplitudes in a full-fledged calculation of top-quark pair production and decay is work in progress.

The full set of results of this paper is available at: https://git.rwth-aachen.de/mczakon/PolarizedTTNNLO.

Acknowledgments

L. Chen acknowledges support by a scholarship from the China Scholarship Council (CSC). R. Poncelet was supported by the Deutsche Forschungsgemeinschaft through Graduierten-

JHEP03(2018)085

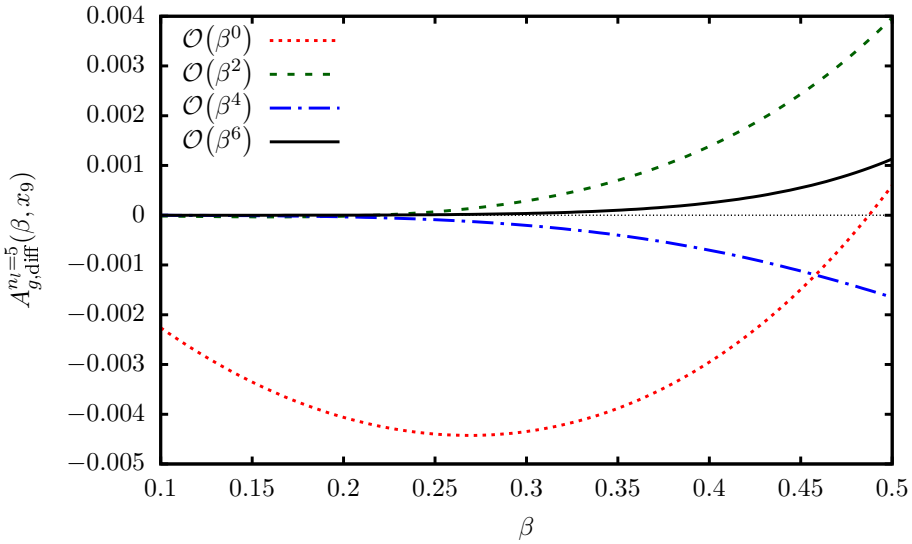

Figure 4. The difference between the threshold expansion for coefficient A_g up to β^n with $n = 0, 2, 4, 6$ and results from numerical integration for a fixed angle θ.

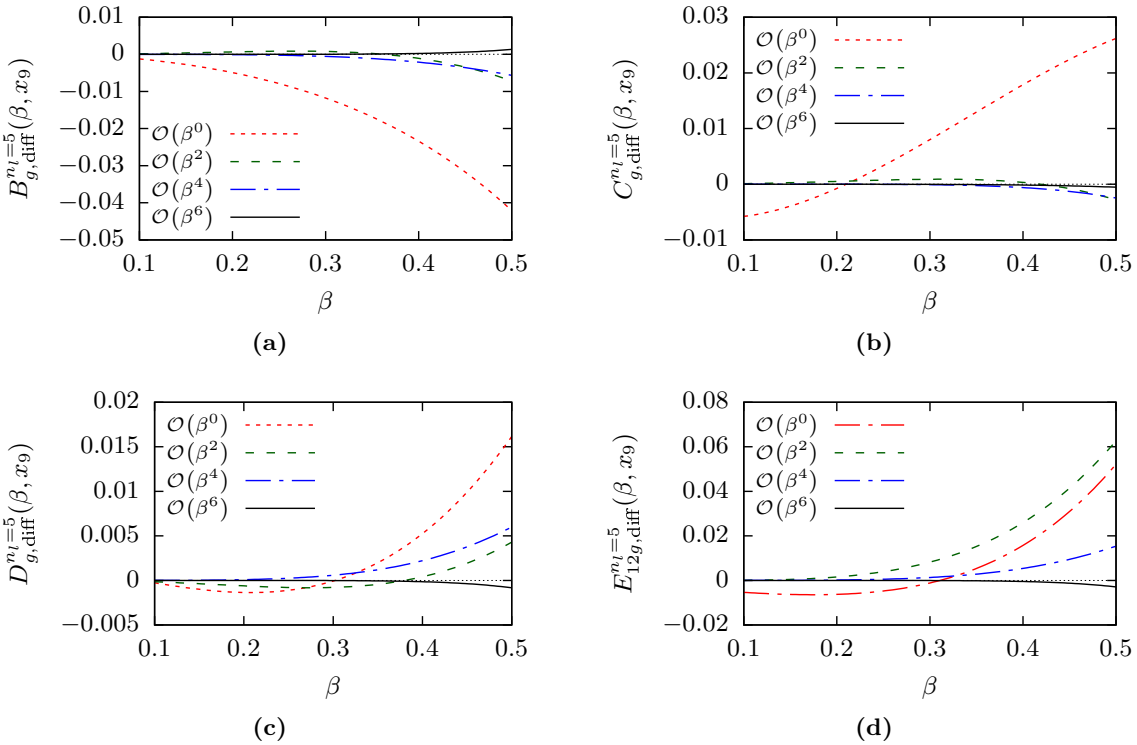

Figure 5. The difference between the threshold expansion for coefficient B_g, C_g, D_g, E_{12g} up to β^n with $n = 0, 2, 4, 6$ and results from numerical integration for a fixed angle θ.

JHEP03(2018)085

kolleg GRK 1675, and in part by the German Research Foundation (DFG) under Grant No. WO 1900/2.

A Renormalization constants and anomalous dimensions

We list all necessary renormalization constants up to the needed power in ϵ. The on-shell renormalization constants are

$$
\begin{aligned}
Z_g &= 1 + \left(\frac{\alpha_s^{(n_f)}}{2\pi}\right) T_F n_h \left\{ -\frac{2}{3\epsilon} - \frac{2}{3} l_\mu - \frac{1}{3}\epsilon l_\mu^2 - \frac{\pi^2}{18}\epsilon - \frac{1}{9}\epsilon^2 l_\mu^3 - \frac{\pi^2}{18}\epsilon^2 l_\mu + \frac{2}{9}\epsilon^2 \zeta_3 \right\} \\
&\quad + \left(\frac{\alpha_s^{(n_f)}}{2\pi}\right)^2 T_F n_h \left\{ T_F n_h \left[\frac{4}{9\epsilon} l_\mu + \frac{2}{3} l_\mu^2 + \frac{\pi^2}{27} \right] + T_F n_l \left[-\frac{4}{9\epsilon^2} - \frac{4}{9\epsilon} l_\mu - \frac{2}{9} l_\mu^2 - \frac{\pi^2}{27} \right] \right. \\
&\quad \left. + C_F \left[-\frac{1}{2\epsilon} - l_\mu - \frac{15}{4} \right] + C_A \left[\frac{35}{36\epsilon^2} + \frac{13}{18\epsilon} l_\mu - \frac{5}{8\epsilon} - \frac{5}{4} l_\mu + \frac{1}{9} l_\mu^2 + \frac{13}{48} + \frac{13\pi^2}{216} \right] \right\},
\end{aligned}
$$

$$
Z_q = 1 + \left(\frac{\alpha_s^{(n_f)}}{2\pi}\right)^2 C_F T_F n_h \left[\frac{1}{4\epsilon} + \frac{1}{2} l_\mu - \frac{5}{24} \right],
$$

$$
\begin{aligned}
Z_Q &= 1 + \left(\frac{\alpha_s^{(n_f)}}{2\pi}\right) C_F \left\{ -\frac{3}{2\epsilon} - 2 - \frac{3}{2} l_\mu - 4\epsilon - 2\epsilon l_\mu - \frac{3}{4}\epsilon l_\mu^2 - \frac{\pi^2}{8}\epsilon - 8\epsilon^2 - 4\epsilon^2 l_\mu - \epsilon^2 l_\mu^2 \right. \\
&\quad \left. - \frac{1}{4}\epsilon^2 l_\mu^3 - \frac{\pi^2}{6}\epsilon^2 - \frac{\pi^2}{8}\epsilon^2 l_\mu + \frac{1}{2}\epsilon^2 \zeta_3 \right\} + \left(\frac{\alpha_s^{(n_f)}}{2\pi}\right)^2 C_F \left\{ T_F n_h \left[\frac{1}{4\epsilon} + \frac{1}{\epsilon} l_\mu + \frac{947}{72} + \frac{11}{6} l_\mu \right. \right. \\
&\quad \left. + \frac{3}{2} l_\mu^2 - \frac{5\pi^2}{4} \right] + T_F n_l \left[-\frac{1}{2\epsilon^2} + \frac{11}{12\epsilon} + \frac{113}{24} + \frac{19}{6} l_\mu + \frac{1}{2} l_\mu^2 + \frac{\pi^2}{3} \right] + C_F \left[\frac{9}{8\epsilon^2} + \frac{51}{16\epsilon} \right. \\
&\quad \left. + \frac{9}{4\epsilon} l_\mu + \frac{433}{32} + \frac{51}{8} l_\mu + \frac{9}{4} l_\mu^2 - \frac{49\pi^2}{16} + 4\ln 2\pi^2 - 6\zeta_3 \right] + C_A \left[\frac{11}{8\epsilon^2} - \frac{127}{48\epsilon} - \frac{1705}{96} \right. \\
&\quad \left. \left. - \frac{215}{24} l_\mu - \frac{11}{8} l_\mu^2 + \frac{5\pi^2}{4} - 2\ln 2\pi^2 + 3\zeta_3 \right] \right\},
\end{aligned}
$$

$$
\begin{aligned}
Z_m &= 1 + \left(\frac{\alpha_s^{(n_f)}}{2\pi}\right) C_F \left\{ -\frac{3}{2\epsilon} - 2 - \frac{3}{2} l_\mu - 4\epsilon - 2\epsilon l_\mu - \frac{3}{4}\epsilon l_\mu^2 - \frac{\pi^2}{8}\epsilon - 8\epsilon^2 - 4\epsilon^2 l_\mu - \epsilon^2 l_\mu^2 \right. \\
&\quad \left. - \frac{1}{4}\epsilon^2 l_\mu^3 - \frac{\pi^2}{6}\epsilon^2 - \frac{\pi^2}{8}\epsilon^2 l_\mu + \frac{1}{2}\epsilon^2 \zeta_3 \right\} + \left(\frac{\alpha_s^{(n_f)}}{2\pi}\right)^2 C_F \left\{ T_F n_h \left[-\frac{1}{2\epsilon^2} + \frac{5}{12\epsilon} + \frac{143}{24} \right. \right. \\
&\quad \left. \left. + \frac{13}{6} l_\mu + \frac{1}{2} l_\mu^2 - \frac{2\pi^2}{3} \right] + T_F n_l \left[-\frac{1}{2\epsilon^2} + \frac{5}{12\epsilon} + \frac{71}{24} + \frac{13}{6} l_\mu + \frac{1}{2} l_\mu^2 + \frac{\pi^2}{3} \right] \right.
\end{aligned}
$$

JHEP03(2018)085

$$+C_F\left[\frac{9}{8\epsilon^2}+\frac{45}{16\epsilon}+\frac{9}{4\epsilon}l_\mu+\frac{199}{32}+\frac{45}{8}l_\mu+\frac{9}{4}l_\mu^2-\frac{17\pi^2}{16}+2\ln 2\pi^2-3\zeta_3\right]$$
$$+C_A\left[\frac{11}{8\epsilon^2}-\frac{97}{48\epsilon}-\frac{1111}{96}-\frac{185}{24}l_\mu-\frac{11}{8}l_\mu^2+\frac{\pi^2}{3}-\ln 2\pi^2+\frac{3}{2}\zeta_3\right]\Bigg\}, \tag{A.1}$$

where $l_\mu = \ln \mu^2/m^2$. The on-shell wave-function renormalization constants for the gluon and light quark fields have been taken from [55, 56].

For the heavy-quark wave-function and mass renormalization constants we used expressions from [57]. The $\overline{\text{MS}}$ renormalization constant for the strong coupling up to $\mathcal{O}\left(\alpha_s^{(n_f)^2}\right)$ is given in terms of beta-function coefficients

$$Z_{\alpha_s} = 1 - \left(\frac{\alpha_s^{(n_f)}}{2\pi}\right)\frac{b_0}{2\epsilon} + \left(\frac{\alpha_s^{(n_f)}}{2\pi}\right)^2\left(\frac{b_0^2}{4\epsilon^2}-\frac{b_1}{8\epsilon}\right), \tag{A.2}$$

where

$$b_0 = \frac{11}{3}C_A - \frac{4}{3}T_F n_f\,, \qquad b_1 = \frac{34}{3}{C_A}^2 - \frac{20}{3}C_A T_F n_f - 4C_F T_F n_f\,. \tag{A.3}$$

The two-loop decoupling constant for the strong coupling is given by [58]

$$\begin{aligned}\zeta_{\alpha_s} &= 1 + \left(\frac{\alpha_s^{(n_l)}}{2\pi}\right)T_F n_h\left\{\frac{2}{3}l_\mu + \frac{1}{3}\epsilon l_\mu^2 + \frac{\pi^2}{18}\epsilon + \frac{1}{9}\epsilon^2 l_\mu^3 + \frac{\pi^2}{18}\epsilon^2 l_\mu - \frac{2}{9}\epsilon^2\zeta_3\right\}\\ &+ \left(\frac{\alpha_s^{(n_l)}}{2\pi}\right)^2 T_F n_h\left\{\frac{4}{9}T_F n_h l_\mu^2 + C_F\left[\frac{15}{4}+l_\mu\right] + C_A\left[-\frac{8}{9}+\frac{5}{3}l_\mu\right]\right\}.\end{aligned} \tag{A.4}$$

The anomalous dimension of the $\mathbf{Z}$ operator used to define the finite remainder function is given by [28]

$$\begin{aligned}\mathbf{\Gamma}_{\mathcal{M}}(\{\underline{p}\},\{\underline{m}\},\mu) &= \sum_{(i,j)}\frac{\mathbf{T}_i\cdot\mathbf{T}_j}{2}\,\gamma_{\text{cusp}}\left(\alpha_s^{(n_l)}\right)\ln\frac{\mu^2}{-s_{ij}} + \sum_i \gamma^i\left(\alpha_s^{(n_l)}\right)\\ &- \sum_{(I,J)}\frac{\mathbf{T}_I\cdot\mathbf{T}_J}{2}\,\gamma_{\text{cusp}}\left(\beta_{IJ},\alpha_s^{(n_l)}\right) + \sum_I \gamma^I\left(\alpha_s^{(n_l)}\right)\\ &+ \sum_{I,j}\mathbf{T}_I\cdot\mathbf{T}_j\,\gamma_{\text{cusp}}\left(\alpha_s^{(n_l)}\right)\ln\frac{m_I\,\mu}{-s_{Ij}}\\ &+ \sum_{(I,J,K)} i\,f^{abc}\,\mathbf{T}_I^a\,\mathbf{T}_J^b\,\mathbf{T}_K^c\,F_1(\beta_{IJ},\beta_{JK},\beta_{KI})\\ &+ \sum_{(I,J)}\sum_k i\,f^{abc}\,\mathbf{T}_I^a\,\mathbf{T}_J^b\,\mathbf{T}_k^c\,f_2\left(\beta_{IJ},\ln\frac{-\sigma_{Jk}\,v_J\cdot p_k}{-\sigma_{Ik}\,v_I\cdot p_k}\right).\end{aligned} \tag{A.5}$$

The lower case indices denote sums over massless particles while capital letters denote sums over massive particles. The brackets $(i,j,\ldots)$ indicate that the sums go over different

JHEP03(2018)085

indicies. The action of the color operator $\mathbf{T}_i^a$ dependence on the type of the parton with index c it acts on. After projecting the result onto the index b we have that in case of a gluon $(\mathbf{T}^a)_{bc} = -if^{abc}$. In case of an outgoing quark (incoming anti-quark) $(\mathbf{T}^a)_{bc} = T^a_{bc}$ and $(\mathbf{T}^a)_{bc} = -T^a_{bc}$ for a incoming quarks (or outgoing anti-quark). For the kinematic dependence we have the definitions

$$s_{ij} = 2\sigma_{ij} p_i p_j + i0^+ \quad \text{with } \sigma_{ij} = +1 \quad \text{if } p_i \text{ and } p_j \text{ in/out going} \quad \text{and} \quad \sigma_{ij} = -1 \text{ otherwise}$$
$$p_I^2 = m_I^2 \qquad v_I = p_I/m_I \qquad \cosh\beta_{IJ} = -s_{IJ}/2m_I m_J \,.$$

In contrast to the spin and color summed case, where all triple color correlators vanish [61], they are essential for the infrared finiteness of the structure coefficients. We also list the anomalous dimensions occurring in eq. (A.5) necessary to obtain the finite remainders of the two-loop amplitudes. The anomalous dimensions related to a single parton (collinear in origin for massless partons and soft in origin for massive partons) are [25, 26]

$$\gamma^g\left(\alpha_s^{(n_l)}\right) = \left(\frac{\alpha_s^{(n_l)}}{2\pi}\right)\left\{-\frac{11}{6}C_A + \frac{2}{3}T_F n_l\right\} + \left(\frac{\alpha_s^{(n_l)}}{2\pi}\right)^2 \left\{{C_A}^2\left[-\frac{173}{27} + \frac{11\pi^2}{72} + \frac{1}{2}\zeta_3\right]\right.$$
$$\left. + C_A T_F n_l\left[\frac{64}{27} - \frac{\pi^2}{18}\right] + C_F T_F n_l\right\}, \tag{A.6}$$

$$\gamma^q\left(\alpha_s^{(n_l)}\right) = -\left(\frac{\alpha_s^{(n_l)}}{2\pi}\right)\frac{3}{2}C_F + \left(\frac{\alpha_s^{(n_l)}}{2\pi}\right)^2 C_F\left\{C_A\left[-\frac{961}{216} - \frac{11\pi^2}{24} + \frac{13}{2}\zeta_3\right]\right.$$
$$\left. + C_F\left[-\frac{3}{8} + \frac{\pi^2}{2} - 6\zeta_3\right] + T_F n_l\left[\frac{65}{54} + \frac{\pi^2}{6}\right]\right\}, \tag{A.7}$$

$$\gamma^Q\left(\alpha_s^{(n_l)}\right) = -\left(\frac{\alpha_s^{(n_l)}}{2\pi}\right)C_F + \left(\frac{\alpha_s^{(n_l)}}{2\pi}\right)^2 C_F\left\{C_A\left[-\frac{49}{18} + \frac{\pi^2}{6} - \zeta_3\right] + \frac{10}{9}T_F n_l\right\}. \tag{A.8}$$

The cusp anomalous dimensions are given by [59, 60]

$$\gamma_{\text{cusp}}\left(\alpha_s^{(n_l)}\right) = \frac{\alpha_s^{(n_l)}}{\pi} + \left(\frac{\alpha_s^{(n_l)}}{2\pi}\right)^2\left\{C_A\left[\frac{67}{9} - \frac{\pi^2}{3}\right] - \frac{20}{9}T_F n_l\right\}, \tag{A.9}$$

$$\gamma_{\text{cusp}}\left(\beta, \alpha_s^{(n_l)}\right) = \gamma_{\text{cusp}}\left(\alpha_s^{(n_l)}\right)\beta\coth\beta$$
$$+ \left(\frac{\alpha_s^{(n_l)}}{2\pi}\right)^2 2C_A\left\{\coth^2\beta\left[\text{Li}_3(e^{-2\beta}) + \beta\,\text{Li}_2(e^{-2\beta}) - \zeta_3 + \frac{\pi^2}{6}\beta + \frac{1}{3}\beta^3\right]\right.$$
$$+ \coth\beta\left[\text{Li}_2(e^{-2\beta}) - 2\beta\ln\left(1 - e^{-2\beta}\right) - \frac{\pi^2}{6}(1+\beta) - \beta^2 - \frac{1}{3}\beta^3\right]$$
$$\left. + \frac{\pi^2}{6} + \zeta_3 + \beta^2\right\}. \tag{A.10}$$

JHEP03(2018)085

The two functions F_1 and f_2 are given by

$$F_1(\beta_{12},\beta_{23},\beta_{31}) = \frac{1}{3}\sum_{I,J,K}^{3}\epsilon_{I,J,K}\frac{\alpha_s}{4\pi}g(\beta_{IJ})\gamma_{\text{cusp}}(\beta_{KI},\alpha_s)\,, \tag{A.11}$$

$$f_2\left(\beta_{12},\ln\frac{-\sigma_{23}v_2p_3}{-\sigma_{13}v_1p_3}\right) = -\frac{\alpha_s}{3\pi}g(\beta_{12})\gamma_{\text{cusp}}(\alpha_s)\ln\left(\frac{-\sigma_{23}v_2p_3}{-\sigma_{13}v_1p_3}\right)\,, \tag{A.12}$$

with the function

$$g(\beta) = \coth\beta\left[\beta^2 + 2\beta\ln\left(1-e^{-2\beta}\right) - \text{Li}_2(e^{-2\beta}) + \frac{\pi^2}{6}\right] - \beta^2 - \frac{\pi^2}{6}\,. \tag{A.13}$$

References

[1] M. Czakon, P. Fiedler and A. Mitov, *Total Top-Quark Pair-Production Cross Section at Hadron Colliders Through $\mathcal{O}(\alpha_S^4)$*, *Phys. Rev. Lett.* **110** (2013) 252004 [arXiv:1303.6254] [INSPIRE].

[2] M. Czakon, D. Heymes and A. Mitov, *High-precision differential predictions for top-quark pairs at the LHC*, *Phys. Rev. Lett.* **116** (2016) 082003 [arXiv:1511.00549] [INSPIRE].

[3] M. Czakon, P. Fiedler, D. Heymes and A. Mitov, *NNLO QCD predictions for fully-differential top-quark pair production at the Tevatron*, *JHEP* **05** (2016) 034 [arXiv:1601.05375] [INSPIRE].

[4] M. Czakon, D. Heymes and A. Mitov, *Dynamical scales for multi-TeV top-pair production at the LHC*, *JHEP* **04** (2017) 071 [arXiv:1606.03350] [INSPIRE].

[5] M. Czakon, D. Heymes, A. Mitov, D. Pagani, I. Tsinikos and M. Zaro, *Top-pair production at the LHC through NNLO QCD and NLO EW*, *JHEP* **10** (2017) 186 [arXiv:1705.04105] [INSPIRE].

[6] M. Czakon, D. Heymes, A. Mitov, D. Pagani, I. Tsinikos and M. Zaro, *The top-quark charge asymmetry at the LHC and Tevatron through NNLO QCD and NLO EW*, arXiv:1711.03945 [INSPIRE].

[7] G. Bevilacqua, M. Czakon, A. van Hameren, C.G. Papadopoulos and M. Worek, *Complete off-shell effects in top quark pair hadroproduction with leptonic decay at next-to-leading order*, *JHEP* **02** (2011) 083 [arXiv:1012.4230] [INSPIRE].

[8] A. Denner, S. Dittmaier, S. Kallweit and S. Pozzorini, *NLO QCD corrections to WWbb production at hadron colliders*, *Phys. Rev. Lett.* **106** (2011) 052001 [arXiv:1012.3975] [INSPIRE].

[9] A. Denner, S. Dittmaier, S. Kallweit and S. Pozzorini, *NLO QCD corrections to off-shell top-antitop production with leptonic decays at hadron colliders*, *JHEP* **10** (2012) 110 [arXiv:1207.5018] [INSPIRE].

[10] A. Denner and M. Pellen, *Off-shell production of top-antitop pairs in the lepton + jets channel at NLO QCD*, *JHEP* **02** (2018) 013 [arXiv:1711.10359] [INSPIRE].

JHEP03(2018)085

[11] G. Bevilacqua, H.B. Hartanto, M. Kraus and M. Worek, *Top Quark Pair Production in Association with a Jet with Next-to-Leading-Order QCD Off-Shell Effects at the Large Hadron Collider*, *Phys. Rev. Lett.* **116** (2016) 052003 [arXiv:1509.09242] [INSPIRE].

[12] G. Bevilacqua, H.B. Hartanto, M. Kraus and M. Worek, *Off-shell Top Quarks with One Jet at the LHC: A comprehensive analysis at NLO QCD*, *JHEP* **11** (2016) 098 [arXiv:1609.01659] [INSPIRE].

[13] M. Brucherseifer, F. Caola and K. Melnikov, $\mathcal{O}(\alpha_s^2)$ *corrections to fully-differential top quark decays*, *JHEP* **04** (2013) 059 [arXiv:1301.7133] [INSPIRE].

[14] J. Gao, C.S. Li and H.X. Zhu, *Top Quark Decay at Next-to-Next-to Leading Order in QCD*, *Phys. Rev. Lett.* **110** (2013) 042001 [arXiv:1210.2808] [INSPIRE].

[15] J. Gao and A.S. Papanastasiou, *Top-quark pair-production and decay at high precision*, *Phys. Rev.* **D 96** (2017) 051501 [arXiv:1705.08903] [INSPIRE].

[16] P. Bärnreuther, M. Czakon and P. Fiedler, *Virtual amplitudes and threshold behaviour of hadronic top-quark pair-production cross sections*, *JHEP* **02** (2014) 078 [arXiv:1312.6279] [INSPIRE].

[17] T. Gehrmann, A. von Manteuffel and L. Tancredi, *The two-loop helicity amplitudes for* $q\bar{q}' \to V_1V_2 \to 4$ *leptons*, *JHEP* **09** (2015) 128 [arXiv:1503.04812] [INSPIRE].

[18] R. Bonciani, A. Ferroglia, T. Gehrmann, D. Maître and C. Studerus, *Two-Loop Fermionic Corrections to Heavy-Quark Pair Production: The Quark-Antiquark Channel*, *JHEP* **07** (2008) 129 [arXiv:0806.2301] [INSPIRE].

[19] R. Bonciani, A. Ferroglia, T. Gehrmann and C. Studerus, *Two-Loop Planar Corrections to Heavy-Quark Pair Production in the Quark-Antiquark Channel*, *JHEP* **08** (2009) 067 [arXiv:0906.3671] [INSPIRE].

[20] R. Bonciani, A. Ferroglia, T. Gehrmann, A. von Manteuffel and C. Studerus, *Two-Loop Leading Color Corrections to Heavy-Quark Pair Production in the Gluon Fusion Channel*, *JHEP* **01** (2011) 102 [arXiv:1011.6661] [INSPIRE].

[21] A. von Manteuffel and C. Studerus, *Massive planar and non-planar double box integrals for light* N_f *contributions to* $gg \to t\bar{t}$, *JHEP* **10** (2013) 037 [arXiv:1306.3504] [INSPIRE].

[22] R. Bonciani, A. Ferroglia, T. Gehrmann, A. von Manteuffel and C. Studerus, *Light-quark two-loop corrections to heavy-quark pair production in the gluon fusion channel*, *JHEP* **12** (2013) 038 [arXiv:1309.4450] [INSPIRE].

[23] S.M. Aybat, L.J. Dixon and G.F. Sterman, *The Two-loop soft anomalous dimension matrix and resummation at next-to-next-to leading pole*, *Phys. Rev.* **D 74** (2006) 074004 [hep-ph/0607309] [INSPIRE].

[24] A. Mitov, G.F. Sterman and I. Sung, *The Massive Soft Anomalous Dimension Matrix at Two Loops*, *Phys. Rev.* **D 79** (2009) 094015 [arXiv:0903.3241] [INSPIRE].

[25] T. Becher and M. Neubert, *On the Structure of Infrared Singularities of Gauge-Theory Amplitudes*, *JHEP* **06** (2009) 081 [*Erratum JHEP* **11** (2013) 024] [arXiv:0903.1126] [INSPIRE].

[26] T. Becher and M. Neubert, *Infrared singularities of QCD amplitudes with massive partons*, *Phys. Rev.* **D 79** (2009) 125004 [*Erratum ibid.* **D 80** (2009) 109901] [arXiv:0904.1021] [INSPIRE].

JHEP03(2018)085

[27] M. Czakon, A. Mitov and G.F. Sterman, *Threshold Resummation for Top-Pair Hadroproduction to Next-to-Next-to-Leading Log*, *Phys. Rev.* **D 80** (2009) 074017 [arXiv:0907.1790] [INSPIRE].

[28] A. Ferroglia, M. Neubert, B.D. Pecjak and L.L. Yang, *Two-loop divergences of massive scattering amplitudes in non-abelian gauge theories*, *JHEP* **11** (2009) 062 [arXiv:0908.3676] [INSPIRE].

[29] A. Mitov, G.F. Sterman and I. Sung, *Computation of the Soft Anomalous Dimension Matrix in Coordinate Space*, *Phys. Rev.* **D 82** (2010) 034020 [arXiv:1005.4646] [INSPIRE].

[30] J.M. Henn, *Multiloop integrals in dimensional regularization made simple*, *Phys. Rev. Lett.* **110** (2013) 251601 [arXiv:1304.1806] [INSPIRE].

[31] R.N. Lee, *Reducing differential equations for multiloop master integrals*, *JHEP* **04** (2015) 108 [arXiv:1411.0911] [INSPIRE].

[32] R.N. Lee and A.A. Pomeransky, *Normalized Fuchsian form on Riemann sphere and differential equations for multiloop integrals*, arXiv:1707.07856 [INSPIRE].

[33] R.N. Lee, A.V. Smirnov and V.A. Smirnov, *Solving differential equations for Feynman integrals by expansions near singular points*, arXiv:1709.07525 [INSPIRE].

[34] O. Gituliar and V. Magerya, *Fuchsia: a tool for reducing differential equations for Feynman master integrals to epsilon form*, *Comput. Phys. Commun.* **219** (2017) 329 [arXiv:1701.04269] [INSPIRE].

[35] M. Prausa, *epsilon: A tool to find a canonical basis of master integrals*, *Comput. Phys. Commun.* **219** (2017) 361 [arXiv:1701.00725] [INSPIRE].

[36] C. Meyer, *Transforming differential equations of multi-loop Feynman integrals into canonical form*, *JHEP* **04** (2017) 006 [arXiv:1611.01087] [INSPIRE].

[37] C. Meyer, *Algorithmic transformation of multi-loop master integrals to a canonical basis with CANONICA*, *Comput. Phys. Commun.* **222** (2018) 295 [arXiv:1705.06252] [INSPIRE].

[38] J.M. Henn, *Lectures on differential equations for Feynman integrals*, *J. Phys.* **A 48** (2015) 153001 [arXiv:1412.2296] [INSPIRE].

[39] L. Adams, E. Chaubey and S. Weinzierl, *Simplifying Differential Equations for Multiscale Feynman Integrals beyond Multiple Polylogarithms*, *Phys. Rev. Lett.* **118** (2017) 141602 [arXiv:1702.04279] [INSPIRE].

[40] M. Caffo, H. Czyz, S. Laporta and E. Remiddi, *The Master differential equations for the two loop sunrise selfmass amplitudes*, *Nuovo Cim.* **A 111** (1998) 365 [hep-th/9805118] [INSPIRE].

[41] S. Laporta and E. Remiddi, *Analytic treatment of the two loop equal mass sunrise graph*, *Nucl. Phys.* **B 704** (2005) 349 [hep-ph/0406160] [INSPIRE].

[42] K.G. Chetyrkin and F.V. Tkachov, *Integration by Parts: The Algorithm to Calculate β-functions in 4 Loops*, *Nucl. Phys.* **B 192** (1981) 159 [INSPIRE].

[43] A.B. Goncharov, *Multiple polylogarithms, cyclotomy and modular complexes*, *Math. Res. Lett.* **5** (1998) 497 [arXiv:1105.2076] [INSPIRE].

[44] E.K. Leinartas, *Factorization of rational functions of several variables into partial fractions*, *Soviet Math.* **22** (1978) 35.

[45] A. Raichev, *Leinartas's partial fraction decomposition*, arXiv:1206.4740.

JHEP03(2018)085

[46] M. Czakon, *Automatized analytic continuation of Mellin-Barnes integrals*, *Comput. Phys. Commun.* **175** (2006) 559 [hep-ph/0511200] [INSPIRE].

[47] H.R.P. Ferguson and D.H. Bailey, *Numerical results on relations between fundamental constants using a new algorithm*, *Math. Comput.* **53** (1989) 649.

[48] S. Moch and P. Uwer, *XSummer: Transcendental functions and symbolic summation in form*, *Comput. Phys. Commun.* **174** (2006) 759 [math-ph/0508008] [INSPIRE].

[49] P.N. Brown, G.D. Byrne and A.C. Hindmarsh, *VODE: A Variable-Coefficient ODE Solver*, *SIAM J. Sci. Stat. Comput.* **10** (1989) 1038.

[50] D.H. Bailey, Y. Hida and X.S. Li, *Quad-double/Double-double Computation Package*, (2017) http://crd.lbl.gov/∼dhbailey/mpdist/.

[51] W. Bernreuther and A. Brandenburg, *Tracing CP-violation in the production of top quark pairs by multiple TeV proton proton collisions*, *Phys. Rev.* **D 49** (1994) 4481 [hep-ph/9312210] [INSPIRE].

[52] P. Bärnreuther, M. Czakon and A. Mitov, *Percent Level Precision Physics at the Tevatron: First Genuine NNLO QCD Corrections to $q\bar{q} \to t\bar{t} + X$*, *Phys. Rev. Lett.* **109** (2012) 132001 [arXiv:1204.5201] [INSPIRE].

[53] M. Czakon and A. Mitov, *NNLO corrections to top-pair production at hadron colliders: the all-fermionic scattering channels*, *JHEP* **12** (2012) 054 [arXiv:1207.0236] [INSPIRE].

[54] M. Czakon and A. Mitov, *NNLO corrections to top pair production at hadron colliders: the quark-gluon reaction*, *JHEP* **01** (2013) 080 [arXiv:1210.6832] [INSPIRE].

[55] M. Czakon, A. Mitov and S. Moch, *Heavy-quark production in massless quark scattering at two loops in QCD*, *Phys. Lett.* **B 651** (2007) 147 [arXiv:0705.1975] [INSPIRE].

[56] M. Czakon, A. Mitov and S. Moch, *Heavy-quark production in gluon fusion at two loops in QCD*, *Nucl. Phys.* **B 798** (2008) 210 [arXiv:0707.4139] [INSPIRE].

[57] D.J. Broadhurst, N. Gray and K. Schilcher, *Gauge invariant on-shell Z_2 in QED, QCD and the effective field theory of a static quark*, *Z. Phys.* **C 52** (1991) 111 [INSPIRE].

[58] W. Bernreuther and W. Wetzel, *Decoupling of Heavy Quarks in the Minimal Subtraction Scheme*, *Nucl. Phys.* **B 197** (1982) 228 [*Erratum ibid.* **B 513** (1998) 758] [INSPIRE].

[59] G.P. Korchemsky and A.V. Radyushkin, *Renormalization of the Wilson Loops Beyond the Leading Order*, *Nucl. Phys.* **B 283** (1987) 342 [INSPIRE].

[60] N. Kidonakis, *Two-loop soft anomalous dimensions and NNLL resummation for heavy quark production*, *Phys. Rev. Lett.* **102** (2009) 232003 [arXiv:0903.2561] [INSPIRE].

[61] M. Czakon and P. Fiedler, *The soft function for color octet production at threshold*, *Nucl. Phys.* **B 879** (2014) 236 [arXiv:1311.2541] [INSPIRE].

JHEP03(2018)085